Check for updates

Geophysical Research Letters

RESEARCH LETTER
10.1029/2026GL122178

The 2 May 2025 Mw 7.4 Drake Passage Earthquake: Insights Into Tectonics at the Shackleton Fracture Zone–Chilean Trench Transition

A. Vuan[1], G. Brancatelli[1], G. Brancolini[1], L. Gasperini[2], R. Geletti[1], E. Lodolo[1], A. Magrin[1], M. Menichetti[3], M. Plasencia[1], A. Polonia[2], M. Santulin[1], and A. Tassone[4]

[1]Istituto Nazionale di Oceanografia e di Geofisica Sperimentale - OGS, Trieste, Italy, [2]Istituto di Scienze Marine - CNR-ISMAR, Bologna, Italy, [3]Dipartimento di Scienze Pure ed Applicate, Università di Urbino, Urbino, Italy, [4]Instituto de Geociencias Básicas, Aplicadas y Ambientales de Buenos Aires (IGeBA), CONICET - Universidad de Buenos Aires, Buenos Aires, Argentina

Key Points:

- Largest instrumentally recorded quake at the transition of the Shackleton Fracture Zone and the Chilean Trench
- Relocated seismicity beneath Drake Passage clusters at 15–35 km depth; the Mw 7.4 mainshock nucleated at 25 km depth on 2 May 2025
- Rupture likely reflects thrust-interface or intraslab faulting with slab-edge deformation at the subduction–strike-slip system transition

Supporting Information:

Supporting Information may be found in the online version of this article.

Correspondence to:

A. Vuan,
avuan@ogs.it

Citation:

Vuan, A., Brancatelli, G., Brancolini, G., Gasperini, L., Geletti, R., Lodolo, E., et al. (2026). The 2 May 2025 Mw 7.4 Drake Passage Earthquake: Insights into tectonics at the Shackleton Fracture Zone–Chilean Trench transition. *Geophysical Research Letters*, *53*, e2026GL122178. https://doi.org/10.1029/2026GL122178

Received 6 FEB 2026
Accepted 1 OCT 2026

Author Contributions:

Conceptualization: A. Vuan, E. Lodolo, A. Polonia
Data curation: A. Vuan, G. Brancolini, L. Gasperini, A. Magrin, M. Menichetti, M. Plasencia, A. Polonia
Formal analysis: A. Vuan, R. Geletti, A. Magrin, M. Santulin
Funding acquisition: A. Vuan
Investigation: A. Vuan, G. Brancolini, L. Gasperini, R. Geletti, A. Polonia, M. Santulin, A. Tassone
Methodology: A. Vuan, G. Brancatelli, R. Geletti, A. Magrin, M. Santulin
Resources: A. Vuan, A. Tassone

© 2026 The Author(s). Geophysical Research Letters published by Wiley Periodicals LLC on behalf of American Geophysical Union.
This is an open access article under the terms of the Creative Commons Attribution License, which permits use, distribution and reproduction in any medium, provided the original work is properly cited.

Abstract On 2 May 2025, an Mw 7.4 earthquake occurred ~120 km off the southern tip of Tierra del Fuego, at the transition of the Shackleton Fracture Zone and the Chile Trench. This event exhibits reverse-faulting mechanisms with relatively steeply dipping planes and is the largest recorded along this complex plate boundary. Most aftershocks have similar mechanisms, although some show strike-slip and normal faulting. To better resolve the activated fault system under limited station coverage, we relocated events and incorporated pP-sP phases identified using a trained classifier to refine focal depths. A multichannel seismic reflection line provides additional insights into the structure of the subduction complex. We infer that the mainshock nucleated on the subduction interface or within the plate of the southernmost Chilean subduction system, with aftershocks marking activation of steeper structures. This behavior emphasizes how convergent and strike-slip fault systems interact to complicate earthquake rupture at plate boundary transitions.

Plain Language Summary On 2 May 2025, a magnitude 7.4 earthquake struck about 120 km off the southern tip of South America near Tierra del Fuego. It was the strongest earthquake ever recorded in this complex region where several tectonic plates meet. The event ruptured a volume separating earlier recorded earthquakes near the junction of major fault systems, none of which exceeded magnitude 6.5. The mainshock and most of the aftershocks showed compressional motion on steeply dipping faults, which is unusual for a typical plate-boundary thrust rupture, and a few showed strike-slip and normal fault motion. Because seismic stations are sparse in this area, advanced methods were used to improve earthquake locations. By identifying depth-sensitive seismic phases with a machine-learning model, we determined that the mainshock began about 25 km deep, consistent with the very small tsunami observed. Aftershocks southeast of the epicenter occurred on west-dipping faults near the Shackleton Fracture Zone. Previously collected seismic imaging data also help illuminate the complex fault system involved.

1. Introduction

The Mw 7.4 earthquake of 2 May 2025 occurred off the southernmost tip of Tierra del Fuego (Figure 1) and represents the strongest event ever documented in this region, where the southern terminus of the South American convergent plate boundary transitions into the Shackleton Fracture Zone (SFZ). The event was interpreted by United States Geological Survey (USGS) as a reverse-faulting earthquake at a depth of 10 km, and the aftershock distribution was described as indicating a rupture propagating southeastward along the SFZ. In the USGS seismic catalog, the sequence associated with the Mw 7.4 mainshock (Figure 1) was preceded by two $M > 6$ earthquakes that occurred in 1975 to the northwest and in 1976 to the southeast. Between 2010 and 2018, several $M > 6$ events ruptured the boundary between the Antarctic and Scotia plates south of the 2025 seismic sequence, reaching the southernmost extent of the 2025 aftershock area. The vast majority of the first day's aftershocks started 45 km SE of the mainshock, and the sequence's largest aftershock, an Mw 6.4, occurred 5 hr later 90 km SE of the epicenter (Figure 1).

The USGS focal mechanism shows a dominantly compressional source, a centroid depth of 23.5 km, and a NW–SE–striking nodal plane dipping either 33° to the northeast or 57° to the southwest, which is unusually steep

Software: A. Vuan, G. Brancatelli
Supervision: A. Vuan, M. Menichetti, A. Polonia
Validation: A. Vuan, G. Brancolini, L. Gasperini, R. Geletti, E. Lodolo, A. Magrin, M. Menichetti, A. Polonia, M. Santulin
Visualization: A. Vuan
Writing – original draft: A. Vuan, E. Lodolo, M. Menichetti, A. Polonia
Writing – review & editing: A. Vuan, E. Lodolo, A. Polonia

for a shallow thrust event along an active subduction zone (Bradley & Hubbard, 2025). In addition, the non–double-couple (NDC) component is anomalously high (37%) (Rösler et al., 2021, 2023), suggesting a complex source process may contribute to this elevated value.

By a finite fault inversion method (Ji et al., 2002), USGS estimated a maximum slip of approximately 4 m. However, this slip distribution is strongly influenced by the use of teleseismic stations located far from the epicentral region, resulting in significant uncertainty. For example, the centroid depth derived from the focal mechanism (23.5 km) is inconsistent with the shallow asperity inferred from the finite-fault model by USGS. Given the complex structural configuration of this segment of the South America margin, where convergence along the Chilean Trench transitions into left-lateral strike-slip deformation along the SFZ (Figure 1 inset), it remains unclear whether the 2025 earthquake primarily reflects subduction-related processes or represents a more complex intraplate event, occurring off the main plate boundary but mechanically related to it.

Transitions from subduction to strike-slip faulting along plate boundaries can be associated with geometric segmentation, termination of the plate interface, block rotations, and changes in relative plate-motion trajectories (Wallace et al., 2012). Overall, this tectonic setting diverges markedly from that of a classic subduction margin, and it remains unclear how, in southernmost South America, Chilean subduction interacts with the SFZ and the associated splay faults to generate large-magnitude earthquakes.

In this study, we analyze seismological data together with a multichannel seismic reflection profile crossing the epicentral area to constrain the 2025 seismic sequence and the shallow crustal architecture of the continental margin off Tierra del Fuego. Epicentral locations of the mainshock and its aftershocks are refined using seismic data from the regional Antarctic Seismographic Argentinean Italian Network (ASAIN) network (Plasencia Linares et al., 2021; Vuan et al., 2000). Hypocentral depths were subsequently investigated through a targeted analysis applied to the mainshock and earlier aftershocks. This was achieved through the application of trained models capable of identifying depth-sensitive seismic phases such as pP and sP. The seismic profile resolves the shallow architecture of the subduction system and offers insights on the location and geometry of the plate interface and major faults potentially involved in the 2025 rupture.

2. Tectonic Setting and Evolution

Structural development offshore southernmost Chile is driven by the relative movements of the Antarctic, Scotia, and South America plates (Figure 1 inset). The boundary between the Scotia and South America plates is defined by the Magallanes–Fagnano fault system and the North Scotia Ridge (Lodolo et al., 2002, 2003), whereas the Antarctic–Scotia plate boundary follows the Chilean Trench to the northwest and the SFZ to the southeast (Figure 1). The Antarctic-South America-Scotia plate triple junction (Fuegian Triple Junction in Figure 1 inset) has been interpreted as a diffuse deformation zone where the Magallanes–Fagnano fault system projects toward the Chilean Trench (Cunningham, 1993; Forsyth, 1975; Polonia et al., 2007). North of this area, subduction involves the Antarctic and South America plates, whereas south of the triple junction, convergence between the Antarctic and Scotia plates becomes progressively more oblique and transitions into the transpressive transcurrent motion of the SFZ.

Post-Miocene plate convergence processes are characterized by subduction between the Antarctic and Scotia plates at a rate of ∼10–20 mm yr^{-1} (DeMets et al., 1990). Seismic reflection profiles reveal strong variations in frontal-wedge morphology, and overall structural style. These variations occur along oblique structural trends that segment the margin, driven by processes on the overriding plate and by local heterogeneities on the incoming plate, such as seamounts, fracture zones, and oceanic fabric (Polonia et al., 2007).

The intra-oceanic SFZ is a northwest–southeast trending fracture zone that extends for over 800 km from the southernmost Chilean Trench to the eastern termination of the South Shetland Trench, where the Antarctic Plate (AP) subducts beneath the South Shetland Islands block (Figure 1 inset) (Aldaya & Maldonado, 1996; Klepeis & Lawver, 1996). Seismicity and focal mechanisms indicate that the SFZ is an active, left-lateral transpressive transcurrent fault zone that accommodates relative motion between the Scotia and APs (Aldaya & Maldonado, 1996; Barker et al., 1991; Galindo-Zaldívar et al., 1996; Klepeis & Lawver, 1996; Livermore et al., 1994; Maldonado et al., 2000; Pelayo & Wiens, 1989). Bathymetric (Bohoyo et al., 2016) and marine seismic data further reveal that the SFZ exhibits pronounced relief, and is flanked to the east by a well-developed trough system (Geletti et al., 2005).

19448007, 2026, 20, Downloaded from https://agupubs.onlinelibrary.wiley.com/doi/10.1029/2026GL122178 by Alessandro Vuan - Ogs Trieste Istituto Nazionale , Wiley Online Library on [13/10/2026]. See the Terms and Conditions (https://onlinelibrary.wiley.com/terms-and-conditions) on Wiley Online Library for rules of use; OA articles are governed by the applicable Creative Commons License

10.1029/2026GL122178

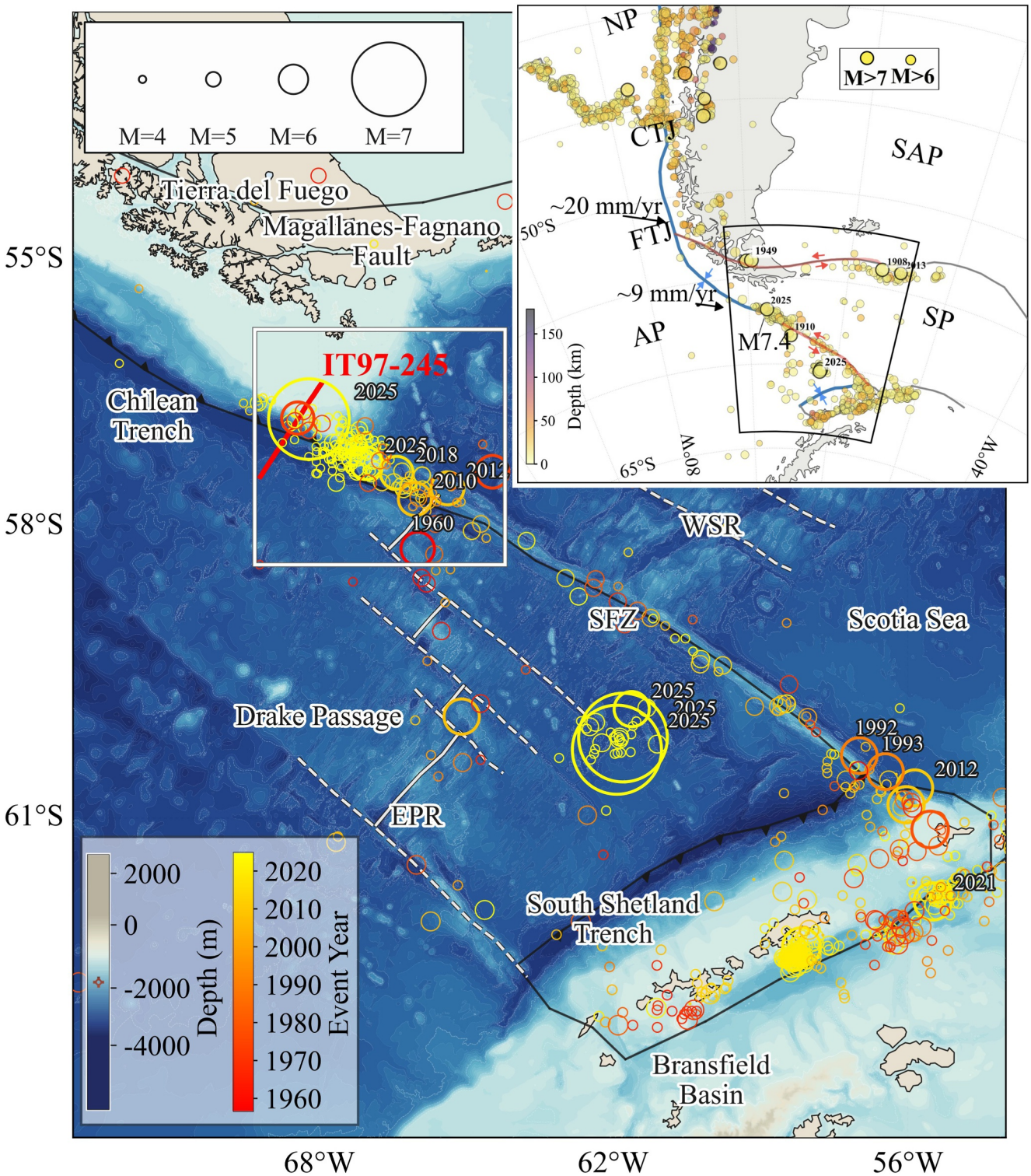


Figure 1.

19448007, 2026, 20, Downloaded from https://agupubs.onlinelibrary.wiley.com/doi/10.1029/2026GL122178 by Alessandro Vuan - Ogs Trieste Istituto Nazionale , Wiley Online Library on [13/10/2026]. See the Terms and Conditions (https://onlinelibrary.wiley.com/terms-and-conditions) on Wiley Online Library for rules of use; OA articles are governed by the applicable Creative Commons License

19448007, 2026, 20, Downloaded from https://agupubs.onlinelibrary.wiley.com/doi/10.1029/2026GL122178 by Alessandro Vuan - Ogs Trieste Istituto Nazionale , Wiley Online Library on [13/10/2026]. See the Terms and Conditions (https://onlinelibrary.wiley.com/terms-and-conditions) on Wiley Online Library for rules of use; OA articles are governed by the applicable Creative Commons License

South of the Chile Triple Junction (Figure 1 inset), seismicity along the margin is low (Pelayo & Wiens, 1989), which may be partly attributed to slow convergence rates and the obliquity of convergence that promotes strain partitioning (Civile et al., 2012; Geletti et al., 2005; Lodolo et al., 2003; Polonia et al., 2007). Strain partitioning does not imply reduced seismicity; rather, it divides deformation between margin-perpendicular thrust faulting and strike-slip faulting on a discrete fault generated by the oblique component of motion, typically localized near the base of the plate interface (McCaffrey et al., 2000). The recorded seismicity in this region is nonetheless insufficient to resolve slab geometry from earthquake data alone. However, seismic reflection profiles indicate that the continental margin between 52°S and 56°S is characterized by large folds and thrust faults (Polonia et al., 1999, 2007). These features suggest that margin-perpendicular shortening is still active, or has slowed only recently (Rubio et al., 2000).

3. Materials and Methods

Our analysis of the 2 May 2025 Drake Passage earthquake sequence integrates regional and teleseismic seismological data with multichannel seismic reflection data. We relocated the mainshock and its aftershocks using high-quality, manually reviewed P- and S-wave arrival times from the Argentine–Italian Antarctic Seismographic Network (ASAIN; Plasencia Linares et al., 2021), supplemented by arrivals from selected global stations (Figure S1; Table S1 in Supporting Information S1). Hypocenters were determined with the LocSAT algorithm (Bratt & Nagy, 1991) using the IASPEI91 global velocity model (Kennett & Engdahl, 1991) (Text S1 in Supporting Information S1).

To better constrain hypocentral depths, we identified pP and sP depth phases using machine-learning tools from the SeisBench framework (Münchmeyer et al., 2023), enabling probabilistic multi-station depth estimation despite sparse regional coverage (see Text S2 and Figure S2 in Supporting Information S1). Focal mechanisms were compiled from multiple international agencies (Dziewonski et al., 1981; Ekström et al., 2012) to assess fault geometry and stress orientation. We further reprocessed a 1997 multichannel seismic reflection profile (Brancatelli et al., 2022; Polonia et al., 2007) crossing the epicentral region to image crustal structure and plate-boundary architecture relevant to the rupture (Figure S3; see Text S3 in Supporting Information S1).

The mean residuals of P-phase arrivals at the most frequently used stations are shown in Figure S4, and Table S2 in Supporting Information S1 summarizes the P- and S-phase data used in the relocation, along with average time residuals, epicentral distances, and azimuths for each station. Stations closest to the events consistently show negative residuals, indicating that observed P arrivals occur earlier than predicted by the velocity model. The major axis of the epicentral uncertainty ellipses is oriented approximately east–west, reflecting sparser station coverage in that direction (Figure S5 in Supporting Information S1). Horizontal location uncertainties range from about 5 km in latitude to 15–20 km in longitude, with reduced longitudinal resolution primarily due to limited station coverage in the Scotia Sea and Pacific Ocean. The systematic residual patterns shown in Figure S4 in Supporting Information S1 are consistent with additional, unmodeled sources of uncertainty (e.g., velocity structure, station geometry) not captured by the formal errors.

Hypocentral depth estimates are improved by incorporating teleseismic depth phases such as pP and sP (Table S6 in Supporting Information S1), although identifying these phases remains challenging due to high ambient noise levels in the region. The robustness of depth phases estimates is evaluated in Figure S6 in Supporting Information S1.

Figure 1. The main map displays shaded bathymetry and topography derived from GEBCO data (GEBCO Bathymetric Compilation Group, 2026), illuminated to emphasize seafloor morphology. Plate boundaries are shown as solid black lines. Earthquakes from the regional catalog are plotted as circles scaled by magnitude and colored by origin time, illustrating the spatiotemporal evolution of seismicity across the Antarctic–Scotia plate boundary. Major tectonic features, including the Chilean Trench, Shackleton Fracture Zone (SFZ), West Scotia Ridge, South Shetland Trench, Bransfield Basin, and Magallanes–Fagnano Fault system, are labeled. The extinct Phoenix Ridge is shown as a white solid line, and transform faults north and south of the SFZ, within the Drake Passage, are shown as white dashed lines. The location of the multichannel seismic profile IT97–245 is indicated by a thick red line, and the white rectangle marks the area enlarged in subsequent figures. Color bars indicate bathymetric depth (m) and event year. In the inset, we show a seismotectonic map of the southern Chile–Scotia Sea plate boundary region, including earthquake epicenters from United States Geological Survey (colored/sized circles). The largest events ($M > 7$) are labeled with year. Circle color indicates hypocentral depth, and size scales with magnitude. The Nazca Plate, the Antarctic Plate, the South America Plate (SAP), and the Scotia Plate are shown and boundaries are traced with colored lines: blue = convergent margin, red = transform/strike-slip boundary. The Chile Triple Junction, where the Nazca, Antarctic, and South America plates meet, and the Fuegian Triple Junction farther south are also labeled. A black-outlined sector delineates the boundaries of the main figure.

19448007, 2026, 20, Downloaded from https://agupubs.onlinelibrary.wiley.com/doi/10.1029/2026GL122178 by Alessandro Vuan - Ogs Trieste Istituto Nazionale , Wiley Online Library on [13/10/2026]. See the Terms and Conditions (https://onlinelibrary.wiley.com/terms-and-conditions) on Wiley Online Library for rules of use; OA articles are governed by the applicable Creative Commons License

4. Results and Interpretation

4.1. Relocated Hypocenters and Depth Distribution

Figure 2 presents cross-sections and map views of seismicity associated with the 2 May 2025 earthquake sequence, combining relocated hypocenters (Table S6 in Supporting Information S1) with pre-mainshock events listed in the ISC-reviewed catalog (Bondár & Storchak, 2011). Relocated hypocenters (red) and background seismicity from the International Seismological Centre (ISC) catalog (orange) are projected onto three vertical cross-sections oriented perpendicular to the mainshock strike and aftershock trend, providing a first-order constraint on the seismogenic geometry of the region.

The inset of Figure 2 reveals a NW–SE elongated seismic cluster centered near 57.3°S, 67.5°W, tightly associated with the Mw 7.4 mainshock. Moving southward, after the mainshock the aftershock activity is visible as an oblique structural lineament trending toward the southeast, starting 45 km south of the mainshock and ending near the position of the largest aftershock, an Mw 6.4 event on the SFZ 90 km south of the mainshock. Its location is at one corner of an approximately equilateral triangle with a cluster of 15+ $M > 5$ events between 2007 and 2018 where the extinct Phoenix-Antarctic spreading ridge (extinct Phoenix Ridge in Figure 1) transitions into the SFZ. The base of this triangle is perpendicular to the SFZ and its other two corners are the 1976, Mw 6.4 earthquake and an Mw 7.1 event.

Backprojection analysis of P-phase data from the Global Seismographic Network (GSN) reveals a complex rupture pattern (EarthScope DS, 2011). The animation shows multiple peaks in beam-power at low frequencies, indicating radiated energy across a broad region spanning the transition zone between the southernmost Chilean Trench and the SFZ, and extending southwestward from the SFZ. Energy release continued for up to 100 s after the origin time. The spatial distribution of these beam-power peaks during coseismic rupture encompasses the locations of early aftershocks.

Figure 2 cross sections A–A1 (aligned with seismic line IT97-245), B–B1, and C–C1 sample this geometry at different latitudes, enabling a three-dimensional characterization of the seismicity. Most hypocenters are located between 0 and 40 km depth, with a clear concentration between ∼10 and ∼30 km. Profile D–D1 (panel d) shows the along-strike distribution of both relocated and ISC events over a distance of approximately 400 km, with depths consistently shallower than 40 km. Relocated events tend to form a tighter cluster approximately 50 km south of the mainshock and are generally better constrained spatially. In contrast, ISC catalog events are more scattered, particularly in the along-strike D–D1 profile, likely reflecting larger catalog location uncertainties. It should be noted that residual location uncertainties, even after relocation, can bias the apparent geometry of seismicity in cross-section; the alignments identified below should therefore be interpreted as first-order trends rather than precisely resolved planes. Nevertheless, in Figures 2b and 2c (profiles B–B1 and C–C1), the seismicity outlines a plane dipping approximately 60° toward the southwest.

Few aftershocks are relocated along profile A–A1, and two of these are very shallow (depth <5 km). Very few aftershocks lie north of the mainshock. An ISC event from 1975 (mb 6.1; Figure 2a) represents the largest earthquake located near the 2025 mainshock. The Mw 7.4 mainshock plots at a depth of approximately ∼25 km, consistent with rupture on the subduction interface or within a subducting plate. The improved aftershock locations obtained in this study reveal a more coherent subsurface geometry that is not apparent from the ISC catalog alone.

Depth is the parameter most sensitive to network geometry: it trades off strongly with origin time and velocity structure when few nearby stations are available, particularly when no stations are close to the earthquake. Without close-in stations or clear depth phases (pP, sP), large depth errors are common. Figure S7 in Supporting Information S1 shows the likelihood distributions and depth estimates for each event, obtained using the trained models (Münchmeyer et al., 2023) described in the Materials and Methods section. Individual 68% credible intervals are spanning 20 km. Even accounting for this substantial per-event uncertainty, most aftershocks cluster tightly between 19 and 34 km, with a median around 26–29 km, and the mainshock falls within this same range. This depth range explains the very small observed tsunami, since deeper rupture produces comparatively little vertical seafloor displacement.

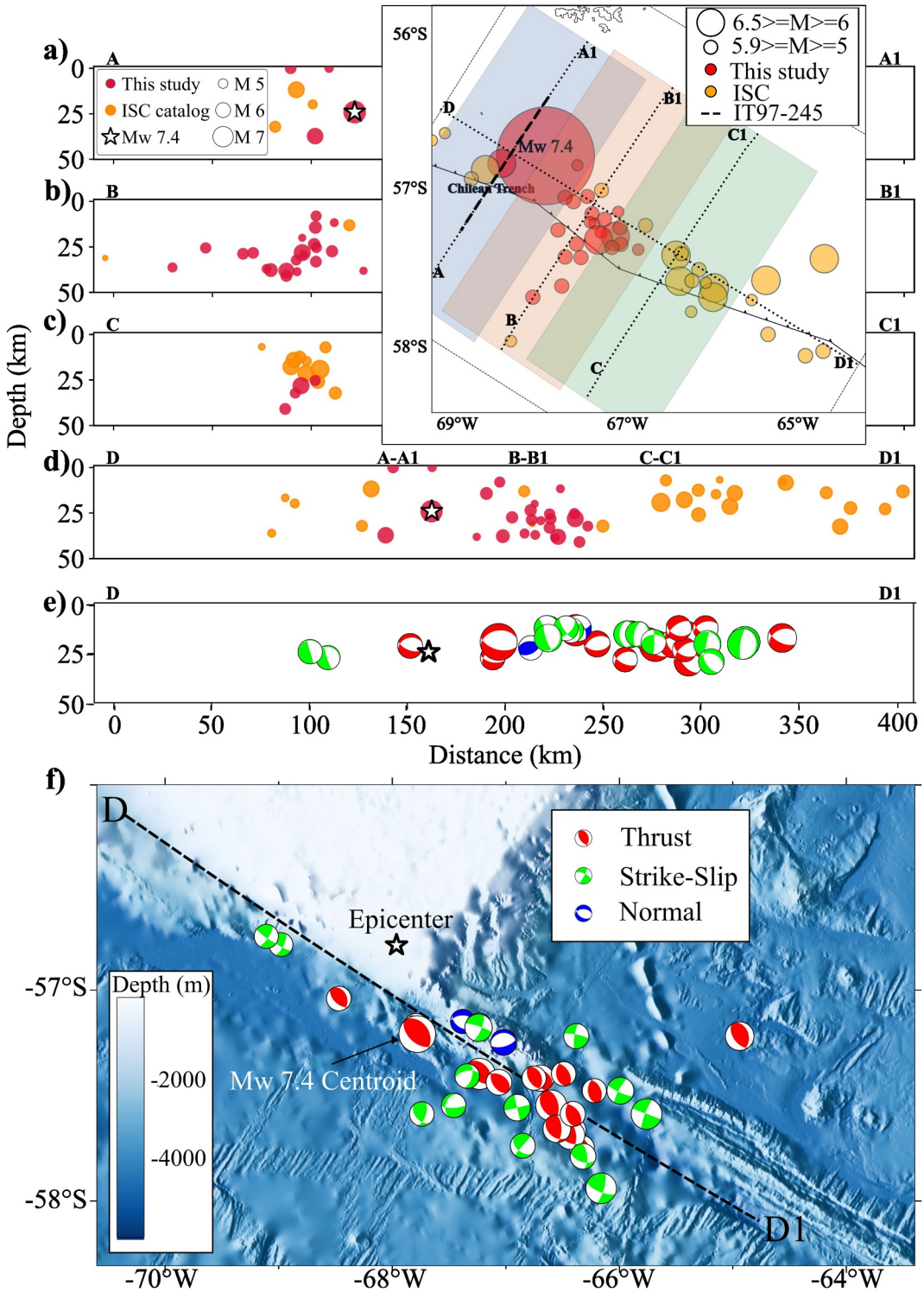


Figure 2.

19448007, 2026, 20, Downloaded from https://agupubs.onlinelibrary.wiley.com/doi/10.1029/2026GL122178 by Alessandro Vuan - Ogs Trieste Istituto Nazionale , Wiley Online Library on [13/10/2026]. See the Terms and Conditions (https://onlinelibrary.wiley.com/terms-and-conditions) on Wiley Online Library for rules of use; OA articles are governed by the applicable Creative Commons License

19448007, 2026, 20, Downloaded from https://agupubs.onlinelibrary.wiley.com/doi/10.1029/2026GL122178 by Alessandro Vuan - Ogs Trieste Istituto Nazionale , Wiley Online Library on [13/10/2026]. See the Terms and Conditions (https://onlinelibrary.wiley.com/terms-and-conditions) on Wiley Online Library for rules of use; OA articles are governed by the applicable Creative Commons License

4.2. Mainshock and Aftershock Mechanisms

The striking heterogeneity in focal mechanisms across the region (Figures 2e and 2f) is described by three populations that are distinguishable at different depths: (a) a shallower group (5–15 km) likely associated with upper plate or interface events near the SFZ, whose focal mechanisms vary considerably showing normal, strike-slip or compressional faulting; (b) strike-slip mechanisms at around 15–20 km; (c) a slightly deeper group (20–30 km), including the mainshock, more consistent with compressional interface seismicity. Some mechanism heterogeneity may reflect the small aftershock fault planes sampling a heterogeneous strain field with many small, variably oriented faults.

Near the A–A1 profile (closest to the mainshock epicenter), mechanisms are thrust to oblique-thrust, consistent with convergence. Centroid depth reported across Global Centroid Moment Tensor (GCMT) and USGS catalogs (Table S3 in Supporting Information S1) agree, the dips of the possible fault planes in the GCMT and USGS solutions appear to be well constrained, as does the compressive orientation of the rupture.

For the mainshock, the two nodal planes indicate dips of approximately 33° and 55° (Figure 2f), steeper than the ∼5°–20° dip expected for the shallow Chilean subduction interface. Analysis of focal mechanisms from the GCMT catalog since 1976 shows that dip angles in this region are consistently greater than 30° (Table S4 in Supporting Information S1). Similarly, Pelayo and Wiens (1989) reported two mb > 6.0 earthquakes in 1975 and 1976 with compressional mechanisms and dips exceeding 30°. Early aftershocks exhibit variable mechanisms including strike-slip with centroid depths of approximately 15 km (Table S5 in Supporting Information S1). Rose diagrams of P-axes (orientations ∼45°–60°, maximum compression) and T-axes (∼135°–150°, maximum tension) derived from these focal solutions are shown in Figure S8 in Supporting Information S1. Temporal and spatial variations of dip angles from GCMT focal mechanisms in the study area are shown in Figure S9 in Supporting Information S1.

4.3. Seismic Reflection Profile and Crustal Structure

The seismic profile runs roughly orthogonal to the margin (Figure 2, inset), crossing the southernmost Chilean subduction complex from the trench to the continental shelf, near the epicenter of the 2 May 2025 earthquake (Figure 3a). The Antarctic–Scotia plate boundary region is imaged to approximately 14 s two-way travel time (TWT), although resolution below 9 s TWT is limited by poor seismic penetration within the deformed accretionary wedge and by the presence of seafloor multiples.

In the oceanic domain to the southwest (0–30 km in Figure 3a), the Antarctic oceanic basement dips landward at approximately 5°. The oceanic crust is underlain by the Moho reflector, imaged at ∼2.5 s TWT below the top of the oceanic basement (Figure 3a). A wedge-shaped sedimentary infill is observed at the trench axis, reaching a thickness of about 2 s TWT near the outer deformation front (Figure 3a). Subvertical faults with small offsets deform AP sediments at the toe of the accretionary wedge (Figure 3a). This geometry suggests incipient deformation, with blind reverse faults that do not reach the seafloor, possibly because sedimentation rates exceed tectonic deformation rates.

The accretionary wedge is ∼20 km wide and consists of deformed sediments up to 5–6 s TWT, scraped off the subducting AP and accreted along landward-dipping thrust faults. Large-scale folds are controlled by reverse faults that terminate at 7–8 s TWT, dip landward at angles between 7° and 13° and steepen toward the northeast.

Figure 2. Spatial and focal-mechanism characterization of the seismicity associated with the 2 May 2025 M_w 7.4 earthquake. The top-right inset shows the epicentral distribution of seismicity relative to the Chilean Trench and the Shackleton Fracture Zone. Circles are scaled by magnitude and colored by data source, red for events relocated in this study, orange for past events from the International Seismological Centre (ISC) catalog. The M_w 7.4 mainshock is shown as a red circle scaled to its magnitude. The black dashed line labeled IT97-245 marks the trace of a reflection seismic line used for structural reference. The four shaded bands (blue, orange, olive, white) delimit the perpendicular and along-strike swath volumes used to select events for cross-sections A–A1, B–B1, C–C1, and D–D1, respectively; dotted lines mark swath boundaries and profile endpoints (a)–(c) Depth cross-sections (0–50 km) along A–A1, B–B1, and C–C1 (traces and swath widths shown in the inset map), showing relocated seismicity (red, this study) and ISC catalog events (orange), scaled by magnitude. The star in (a) marks the M_w 7.4 mainshock. (d) Composite along-strike depth section (0–50 km) combining seismicity from all events projected onto D–D1. (e) Along-strike D–D1 depth section (0–50 km vs. distance, km) showing focal mechanisms color-coded by faulting style. (f) High-resolution shaded bathymetry and topography derived from GEBCO data (GEBCO Bathymetric Compilation Group, 2026), and map-view of focal mechanisms along profile D–D1, color-coded as in (e) and scaled by magnitude.

10.1029/2026GL122178

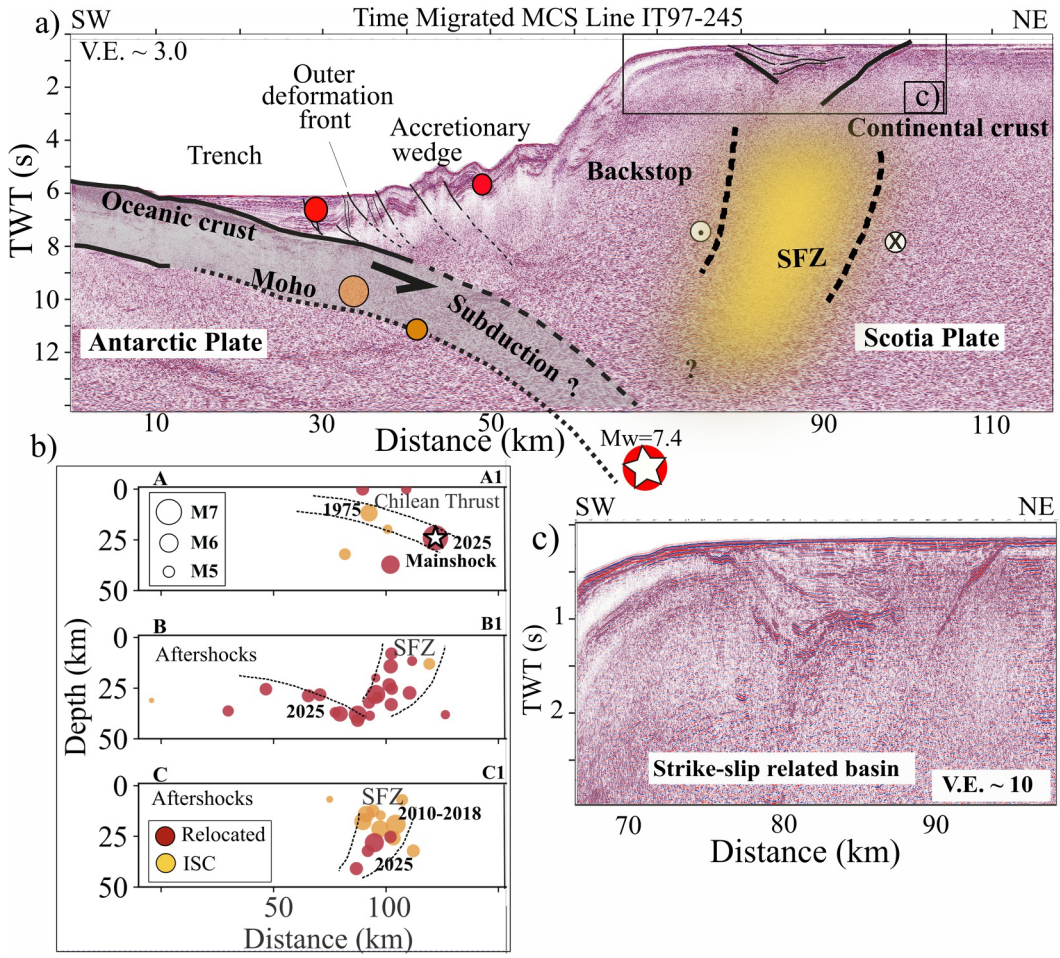


Figure 3. Multichannel seismic reflection data and earthquake distribution across the southernmost Chilean margin at the transition to the Shackleton Fracture Zone (SFZ). (a) Time-migrated multichannel seismic (MCS) profile IT97-245 oriented approximately SW–NE (location shown in Figure 2), crossing the Chilean Trench, accretionary wedge, backstop, and continental crust (Scotia Plate). The section is displayed in two-way travel time (TWT) with a vertical exaggeration of ~3. The Antarctic oceanic crust dips landward beneath the margin and is underlain by a Moho reflection. A wedge-shaped sedimentary infill is observed at the trench axis, and the accretionary prism consists of landward-dipping thrust sheets rooted in a shallow-dipping main detachment (7–13°). High-angle faults deform sediments at the toe of the accretionary wedge. The inferred downdip continuation of the subduction interface and the deformation zone associated with the SFZ are indicated schematically. Projected hypocenters include the Mw 7.4 mainshock (star), relocated aftershocks (red circles), and International Seismological Centre (ISC) catalog events (orange circles). (b) Vertical sections A–A′, B–B′, and C–C′ showing relocated earthquakes (red symbols) and ISC events (orange symbols) projected onto profiles oriented parallel and oblique to the margin. Relocated hypocenters, which are naturally in depth, not TWT, can be plotted on the same axes as the reflection data. Symbol size scales with magnitude. Section A–A′ follows the seismic line and samples the mainshock vicinity, B–B′ illustrates seismicity distributed between the subduction interface and a steep SW-dipping structure, and C–C′ highlights aftershocks aligned along the northern termination of the SFZ. Depths are relative to sea level. (c) Detail of the continental-shelf portion of the MCS profile highlights a well-developed sedimentary basin associated with the strike-slip deformation of the SFZ. This basin coincides with the projection of the aftershock cluster and provides structural evidence for transpressive transcurrent faulting within the continental crust (vertical exaggeration ~10).

A well-developed sedimentary basin is imaged beneath the continental shelf (Figure 3c). The basin depocenter contains a sedimentary succession approximately 2 s TWT thick (corresponding to about 1,000 m, assuming a seismic velocity of 2,000 m s^{-1}). The location of this basin coincides with the northwestward continuation of the SFZ, suggesting that the SFZ exerts a first-order control on the tectonic evolution of the region.

If the main detachment surface is extrapolated northeastward, and the continuation of the SFZ is taken into account as shown in Figure 3a, we propose that the southernmost Chilean convergent plate boundary transitions

19448007, 2026, 20, Downloaded from https://agupubs.onlinelibrary.wiley.com/doi/10.1029/2026GL122178 by Alessandro Vuan - Ogs Trieste Istituto Nazionale , Wiley Online Library on [13/10/2026]. See the Terms and Conditions (https://onlinelibrary.wiley.com/terms-and-conditions) on Wiley Online Library for rules of use; OA articles are governed by the applicable Creative Commons License

into the SFZ deformation zone at a depth of approximately 25 km, corresponding to the nucleation depth of the earthquake (Figure 3a).

The three vertical sections in Figures 3b–3d provide insights into earthquake distribution relative to the geometry of the main faults reconstructed along the seismic line. Section A—A1 runs along the seismic profile and crosses near the mainshock. Two earthquakes are distributed within the lower plate, the mainshock and two earthquakes from the ISC catalog are located along the subduction interface, and two shallow earthquakes correspond to thrust faults within the accretionary prism. In this region, no earthquakes are associated with steep faults in the continental crust. Section B—B1, located farther south, shows seismicity distributed between two structures: one gently dipping toward the NE and the other more steeply dipping toward the SW. At these latitudes, the rupture appears to have affected both the subduction thrust and the northern termination of the SFZ. Section C-C1, located across the SFZ in the southernmost part of the sequence, shows seismicity aligned along a steep structure dipping toward the SW.

5. Discussion

The epicentral region of the Mw 7.4 mainshock is located at the transition between the southernmost Chilean Trench and the SFZ (Figure 1). Along the trench, convergence velocities decrease southward, from 20 mm/yr at 51°S to 9 mm/yr at 56°S (DeMets et al., 1990; Thomas et al., 2003), while subduction becomes increasingly oblique. Similar oblique-convergence settings occur along the New Zealand Hikurangi-Alpine Fault system (Stevens et al., 2024), in Sumatra, where the right-lateral Great Sumatran Fault accommodates oblique Indo-Australian/Eurasian convergence (McNeill & Henstock, 2014; Moeremans et al., 2014), and at the Australian-Pacific boundary close to the Macquarie Triple Junction in the SW-Pacific Ocean (Gasperini et al., 2022).

Despite the low convergence rates, a narrow, well-defined accretionary prism has developed at the toe of the backstop (Figure 3a). Active thrust faults at the transition between the subduction system and the oceanic domain indicate ongoing compressional deformation, implying that the thrust may still be accommodating plate motion.

Fault-plane solutions indicate a reverse mechanism for the 2 May 2025 mainshock, with NE- or SW-dipping nodal planes at 30–35° or 55–60°, respectively. On the seismic profile (Figure 3a), the thrust appears as a high-amplitude reflector dipping at 7–13° that steepens northeastward, although poor penetration prevents identification of the basal detachment landward of 45 km. Interpolation of the thrust interface from the well-imaged outer wedge to the hypocenter suggests a NE dip of up to 25–30°. In contrast, the SFZ is only inferred here, since no reflector is observed at depth; the main evidence is a sedimentary basin at 80–100 km along the profile, connected to the source area, implying a SW-dipping structure with a dip of 60–80° (Figure 3c).

The three vertical sections in Figure 3b show the mainshock nucleation at the base of the accretionary prism, at the contact with the backstop, where the two principal structures accommodating plate motion interact. Southward, the larger aftershock occurred 5 hr after the mainshock extending seismicity along the transition of the Chilean Trench with the SFZ. Focal mechanisms indicate two complementary geometries: (a) reverse faulting consistent with the subducting slab interface, and (b) higher-angle (55–60°) reverse faulting compatible with a southwest-dipping plane.

Using scaling relations specifically derived for subduction interface or intraslab earthquakes (Strasser et al., 2010), we obtain median estimates of approximately 70–80 km in length and 40–45 km in width. This scaling of fault length implies that the mainshock rupture most likely involved the area occupied by the earliest, southernmost aftershocks.

Backprojection of P-wave data from the GSN (EarthScope DS, 2011), reveals multiple low-frequency beam-power peaks propagating across the trench-SFZ transition zone and southwestward along the SFZ, with bursts of energy release continuing up to 100 s after origin time. These peaks overlap early aftershocks, indicating that the mainshock rupture was not confined to a single, simply dipping plane. Thus, interpreting the 30° nodal plane as a direct proxy for the main thrust is complicated by evidence that the rupture was more spatially extended than a single-plane source implies.

This complexity bears directly on how the steep (30–35°) nodal plane at 25 km depth should be interpreted. Two scenarios remain equally consistent with the data: an interface-hosted rupture, and an intraslab rupture decoupled from interface geometry. Under the first, the mainshock would reflect slip on the plate interface itself, with the

19448007, 2026, 20, Downloaded from https://agupubs.onlinelibrary.wiley.com/doi/10.1029/2026GL122178 by Alessandro Vuan - Ogs Trieste Istituto Nazionale , Wiley Online Library on [13/10/2026]. See the Terms and Conditions (https://onlinelibrary.wiley.com/terms-and-conditions) on Wiley Online Library for rules of use; OA articles are governed by the applicable Creative Commons License

19448007, 2026, 20, Downloaded from https://agupubs.onlinelibrary.wiley.com/doi/10.1029/2026GL122178 by Alessandro Vuan - Ogs Trieste Istituto Nazionale , Wiley Online Library on [13/10/2026]. See the Terms and Conditions (https://onlinelibrary.wiley.com/terms-and-conditions) on Wiley Online Library for rules of use; OA articles are governed by the applicable Creative Commons License

nodal plane representing a locally steepened segment of a dipping thrust. A comparable geometry occurs well north of the study area along the southern-to-south-central Chilean margin (41.5°S–43.5°S), where the shallow Wadati-Benioff zone dips at 20–30°, seismicity occurs in a coast-parallel belt at 12–30 km depth, and stress-field rotation is controlled by slab geometry rather than uniform interface dip (Haberland et al., 2006; Lange et al., 2007). This analog shows that steep, segmented interface geometries are not unusual along the Chilean margin, lending plausibility to a similar mechanism here. Under the second, the mainshock instead reflects faulting within subducted oceanic crust. The northernmost portion of the SFZ is a three-dimensional zone where deformation cannot remain confined to a single thrust. Slab-edge bending and tearing, together with slab-window thermal effects, could redistribute stress broadly (Furlong & Schwartz, 2004; Govers & Wortel, 2005). This can produce reverse to oblique-reverse faulting within the slab while strike-slip motion partitions onto the northernmost SFZ segments, generating steep nodal planes at depth independent of subduction interface dip.

The data cannot resolve which of these scenarios applies: both are consistent with the geometrically complex character of this corner, and the focal solutions alone cannot discriminate between them. Rupture of a steep (60°) compressional structure within the continental backstop, while mechanically possible, appears less likely as the primary source, given the expected slip and rupture length.

This hierarchical interaction, a lower-angle, interface-compatible or intraslab source overlain by higher-angle southwest-dipping structures, provides a coherent framework for the spatial pattern of seismicity and variability of focal mechanisms across this segment of the Chile Trench-SFZ transition, though resolving the remaining ambiguity would require additional constraints that the region's remoteness currently limits.

6. Conclusions

Relocated hypocenters beneath the Drake Passage show that seismicity is concentrated between ∼15 and ∼35 km depth, with consistent results from both deep learning–based and conventional relocation methods. The Mw 7.4 mainshock of 2 May 2025 nucleated at a depth of ∼25 km. Longitude uncertainties are larger (∼5–20 km) because of sparse station coverage in this remote area, but depth estimates constrained by pP and sP phases are consistent with ISC-reviewed events near the aftershock zone. The depth distribution of the mainshock and aftershocks, the beam-power peaks from backprojection, the variability in focal mechanisms, and fault geometry from multichannel seismic reflection data suggest a composite rupture involving different fault segments. We propose two possible scenarios at the transition between the southernmost Chilean subduction interface and the SFZ: a thrust interface-hosted and an intraslab rupture. Both scenarios could involve slab-edge deformation with broad redistribution of stress. These results highlight the role of interacting convergent and strike-slip tectonic systems in controlling large earthquake rupture processes at plate boundary transitions.

Conflict of Interest

The authors declare no conflicts of interest relevant to this study.

Availability Statement

All data used in this study are publicly available and properly cited in the references and Supporting Information S1.

Waveform and metadata used for event relocation were obtained from the ASAIN seismic network (Plasencia Linares et al., 2021) and selected FDSN global stations (see Table S1 and Figure S1 in Supporting Information S1 for station list and usage details). Data can be accessed at the EarthScope Data Center (IRIS DMC): https://service.earthscope.org/fdsnws/dataselect/1/, the ORFEUS Data Center (ORFEUS): http://www.orfeus-eu.org/fdsnws/dataselect/1/, and GEOFON web service client (https://geofon.gfz.de/waveform/webservices/). ObsPy package version 1.4 (Krischer et al., 2015) is used to download data.

Regional catalog and focal–mechanism data prior to the mainshock were obtained from the ISC (International Seismological Centre, 2026).

Global Centroid Moment Tensor solutions were retrieved from http://www.globalcmt.org.

19448007, 2026, 20, Downloaded from https://agupubs.onlinelibrary.wiley.com/doi/10.1029/2026GL122178 by Alessandro Vuan - Ogs Trieste Istituto Nazionale , Wiley Online Library on [13/10/2026]. See the Terms and Conditions (https://onlinelibrary.wiley.com/terms-and-conditions) on Wiley Online Library for rules of use; OA articles are governed by the applicable Creative Commons License

Source parameters and centroid solutions for the 2 May 2025 Drake Passage mainshock (Mw 7.4) were accessed from the USGS Earthquake Event Page http://earthquake.usgs.gov/earthquakes/eventpage/us7000pwkn (last access 9 July 2026).

Seismic reflection data along line IT97–245 were reprocessed using Echos and Geodepth software from Aspen Technology (https://www.aspentech.com/en/products/sse/aspen-echos, https://www.aspentech.com/en/products/sse/aspen-geodepth); interpreted and uninterpreted seismic sections are provided as Figure 3 and Figure S3 in Supporting Information S1.

Software used for routine processing includes SeisComP (GFZ & Gempa GmbH, 2008). SeisComP relocation parameters are provided in Table S2 in Supporting Information S1.

Depth–phase identification employed the SeisBench (Woollam et al., 2022) software and deep–learning models (Münchmeyer et al., 2023) and available at (Münchmeyer et al., 2021). The derived relocated catalog is provided as Table S6 in Supporting Information S1.

All resources above are openly available or preserved in trusted repositories with persistent identifiers, in accordance with AGU policy requiring that data and code needed to understand, evaluate, and build upon the results be accessible at the time of review and publication.

Acknowledgments

We thank the Associate Editor German Prieto, Dr. Anouk Beniest and an anonymous reviewer for insightful comments that helped clarify several key aspects and significantly improve the overall quality of the manuscript. We thank the institutions and data providers that made this research possible. Seismic data were provided by the ASAIN and the ISC. This work was supported by the Italian Programma Nazionale di Ricerche in Antartide (PNRA). We thank A. Camerlenghi for enabling the acquisition of the seismic line during the return from the Antarctic Peninsula, which took place over several days of fair weather, a rare condition at these latitudes. The authors acknowledge the scientific and logistic support of Dirección Nacional del Antártico (DNA)—Instituto Antártico Argentino (IAA) and the fundamental role of the Armada, Ejército, and Fuerza Aérea Argentina personnel in creating and maintaining the proper operating conditions for the ASAIN stations at the Antarctic bases.

References

Aldaya, F., & Maldonado, A. (1996). Tectonics of the triple junction at the southern end of the Shackleton Fracture Zone (Antarctic Peninsula). *Geo-Marine Letters*, *16*(4), 279–286. https://doi.org/10.1007/BF01245558

Barker, P. F., Dalziel, I. W. D., & Storey, B. C. (1991). Tectonic development of the Scotia Arc region. In R. J. Tingey (Ed.), *The geology of Antarctica* (pp. 215–248). Clarendon Press.

Bohoyo, F., Larter, R. D., Galindo-Zaldívar, J., Leat, P. T., Maldonado, A., Tate, A. J., et al. (2016). *Bathymetry and geological setting of the Drake Passage (BAS GEOMAP 2 Series)*. British Antarctic Survey.

Bondár, I., & Storchak, D. A. (2011). Improved location procedures at the international seismological centre. *Geophysical Journal International*, *186*(3), 1220–1244. https://doi.org/10.1111/j.1365-246X.2011.05107.x

Bradley, K., & Hubbard, J. (2025). Unusual m7.4 earthquake strikes south of South america. *Earthquake Insights*. https://doi.org/10.62481/0b850b61

Brancatelli, G., Forlin, E., Bertone, N., Del Ben, A., & Geletti, R. (2022). Chapter 7 - Time to depth seismic reprocessing of vintage data: A case study in the Otranto Channel (South Adriatic Sea). In R. Bell, D. Iacopini, & M. Vardy (Eds.), *Interpreting subsurface seismic data* (pp. 157–197). Elsevier. https://doi.org/10.1016/B978-0-12-818562-9.00009-1

Bratt, S. R., & Nagy, W. (1991). *The LocSAT Program*. (Tech. Rep.) (User manual/report). Science Applications International Corporation (SAIC).

Civile, D., Lodolo, E., Vuan, A., & Loreto, M. F. (2012). Tectonics of the Scotia–Antarctica plate boundary constrained from seismic and seismological data. *Tectonophysics*, *550–553*, 17–34. https://doi.org/10.1016/j.tecto.2012.05.002

Cunningham, W. D. (1993). Strike-slip faults in the southernmost Andes and the development of the Patagonian orocline. *Tectonics*, *12*(1), 169–186. https://doi.org/10.1029/92TC01790

DeMets, C., Gordon, R. G., Argus, D. F., & Stein, S. (1990). Current plate motions. *Geophysical Journal International*, *101*(2), 425–478. https://doi.org/10.1111/j.1365-246X.1990.tb06579.x

Dziewonski, A. M., Chou, T.-A., & Woodhouse, J. H. (1981). Determination of earthquake source parameters from waveform data for studies of global and regional seismicity. *Journal of Geophysical Research*, *86*(B4), 2825–2852. https://doi.org/10.1029/JB086iB04p02825

EarthScope, D. S. (2011). Data Services Products: BackProjection P-wave back-projection rupture imaging [Dataset]. *EarthScope Data Service*. https://doi.org/10.17611/DP/23180094

Ekström, G., Nettles, M., & Dziewonski, A. M. (2012). The global CMT project 2004–2010: Centroid-moment tensors for 13,017 earthquakes. *Physics of the Earth and Planetary Interiors*, *200–201*, 1–9. https://doi.org/10.1016/j.pepi.2012.04.002

Forsyth, D. W. (1975). Fault plane solutions and tectonics of the South Atlantic and Scotia Sea. *Geophysical Journal International*, *80*(11), 1429–1443. https://doi.org/10.1029/JB080i011p01429

Furlong, K. P., & Schwartz, S. Y. (2004). Influence of the mendocino triple junction on the tectonics of coastal California. *Annual Review of Earth and Planetary Sciences*, *32*(1), 403–433. https://doi.org/10.1146/annurev.earth.32.101802.120252

Galindo-Zaldívar, J., Jabaloy, A., Maldonado, A., & Sanz de Galdeano, C. (1996). Continental fragmentation along the South Scotia Ridge transcurrent plate boundary (NE Antarctic Peninsula). *Tectonophysics*, *258*(1–4), 275–301. https://doi.org/10.1016/0040-1951(95)00211-1

Gasperini, L., Ligi, M., Accettella, D., Bosman, A., Cuffaro, M., Lodolo, E., et al. (2022). Late Miocene to recent tectonic evolution of the Macquarie Triple Junction. *Geology*, *51*(2), 146–150. https://doi.org/10.1130/G50556.1

GEBCO Bathymetric Compilation Group. (2026). The GEBCO 2026 Grid - A continuous terrain model for oceans and land at 15 arc-second intervals [Dataset]. *NERC EDS British Oceanographic Data Centre NOC*. https://doi.org/10.5285/4f68d5c7-45eb-f999-e063-7086abc036fa

Geletti, R., Lodolo, E., Schreider, A. A., & Polonia, A. (2005). Seismic structure and tectonics of the Shackleton Fracture Zone (Drake Passage, Scotia Sea). *Marine Geophysical Researches*, *26*(1), 17–28. https://doi.org/10.1007/s11001-005-0147-4

GFZGempa GmbH. (2008). The SeisComP seismological software package [Software]. *GFZ Data Services*. https://doi.org/10.5880/GFZ.2.4.2020.003

Govers, R., & Wortel, M. (2005). Lithosphere tearing at STEP faults: Response to edges of subduction zones. *Earth and Planetary Science Letters*, *236*(1), 505–523. https://doi.org/10.1016/j.epsl.2005.03.022

Haberland, C., Rietbrock, A., Lange, D., Bataille, K., & Hofmann, S. (2006). Interaction between forearc and oceanic plate at the south-central chilean margin as seen in local seismic data. *Geophysical Research Letters*, *33*(23). https://doi.org/10.1029/2006GL028189

International Seismological Centre. (2026). On-line bulletin [Dataset]. *International Seismological Centre*. https://doi.org/10.31905/D808B830

Ji, C., Wald, D. J., & Helmberger, D. V. (2002). Source description of the 1999 Hector Mine, California, earthquake. Part I: Wavelet domain inversion theory and resolution analysis. *Bulletin of the Seismological Society of America*, *92*(4), 1192–1207. https://doi.org/10.1785/0120000916

Kennett, B. L. N., & Engdahl, E. R. (1991). Traveltimes for global earthquake location and phase identification. *Geophysical Journal International*, *105*(2), 429–465. https://doi.org/10.1111/j.1365-246X.1991.tb06724.x

Klepeis, K. A., & Lawver, L. A. (1996). Tectonics of the Antarctic–Scotia plate boundary near Elephant and Clarence Islands, West Antarctica. *Journal of Geophysical Research*, *101*(B9), 20211–20231. https://doi.org/10.1029/96JB01510

Krischer, L., Megies, T., Barsch, R., Beyreuther, M., Lecocq, T., Caudron, C., & Wassermann, J. (2015). ObsPy: A bridge for seismology into the scientific Python ecosystem [Software]. *Computational Science & Discovery*, *8*(1). https://doi.org/10.1088/1749-4699/8/1/014003.014003.

Lange, D., Rietbrock, A., Haberland, C., Bataille, K., Dahm, T., Tilmann, F., & Flüh, E. R. (2007). Seismicity and geometry of the south Chilean subduction zone (41.5°S–43.5°S): Implications for controlling parameters. *Geophysical Research Letters*, *34*(6). https://doi.org/10.1029/2006GL029190

Livermore, R., McAdoo, D., & Marks, K. (1994). Scotia Sea tectonics from high-resolution satellite gravity. *Earth and Planetary Science Letters*, *123*(1–3), 255–268. https://doi.org/10.1016/0012-821X(94)90272-0

Lodolo, E., Menichetti, M., Bartole, R., Ben-Avraham, Z., Tassone, A., & Lippai, H. (2003). Magallanes–Fagnano continental transform fault (Tierra del Fuego, southernmost South America). *Tectonics*, *22*(6), 1076. https://doi.org/10.1029/2003TC001500

Lodolo, E., Menichetti, M., Tassone, A., Geletti, R., Sterzai, P., Lippai, H., & Hormaechea, H.-L. (2002). Researchers target a continental transform fault in Tierra del Fuego. *EOS Transactions of the American Geophysical Union*, *83*(1), 5–61. https://doi.org/10.1029/2002EO000001

Maldonado, A., Carlos Balanyá, J., Barnolas, A., Galindo-Zaldívar, J., Hernández, J., Jabaloy, A., et al. (2000). Tectonics of an extinct ridge-transform intersection, Drake Passage (Antarctica). *Marine Geophysical Researches*, *21*(1–2), 43–68. https://doi.org/10.1023/A:1004762311398

McCaffrey, R., Zwick, P. C., Bock, Y., Prawirodirdjo, L., Genrich, J. F., Stevens, C. W., et al. (2000). Strain partitioning during oblique plate convergence in northern sumatra: Geodetic and seismologic constraints and numerical modeling. *Journal of Geophysical Research*, *105*(B12), 28363–28376. https://doi.org/10.1029/1999JB900362

McNeill, L. C., & Henstock, T. J. (2014). Forearc structure and morphology along the Sumatra–Andaman subduction zone. *Tectonics*, *33*(2), 112–134. https://doi.org/10.1002/2012TC003264

Moeremans, R., Singh, S. C., Mukti, M., McArdle, J., & Johansen, K. (2014). Seismic images of structural variations along the deformation front of the Andaman–Sumatra subduction zone: Implications for rupture propagation and tsunamigenesis. *Earth and Planetary Science Letters*, *386*, 75–85. https://doi.org/10.1016/j.epsl.2013.11.003

Münchmeyer, J., Saul, J., & Tilmann, F. (2023). Learning the deep and the shallow: Deep-learning-based depth phase picking and earthquake depth estimation. *Seismological Research Letters*, *95*(3), 1543–1557. https://doi.org/10.1785/0220230187

Münchmeyer, J., Woollam, J., Rietbrock, A., Tilmann, F., Lange, D., Bornstein, T., et al. (2021). SeisBench: A toolbox for machine learning in seismology [Software]. *Zenodo*. https://doi.org/10.5281/zenodo.5568813

Pelayo, A. M., & Wiens, D. A. (1989). Seismotectonics and relative plate motions in the Scotia Sea region. *Journal of Geophysical Research*, *94*(B6), 7293–7320. https://doi.org/10.1029/JB094iB06p07293

Plasencia Linares, M. P., Cravos, C., Laterza, R., Bernardi, P., Comelli, P., Grossi, M., et al. (2021). The Antarctic Seismographic Argentinean Italian Network (ASAIN): Recording earthquakes in the Scotia Sea Region. *Seismological Research Letters*, *92*(5), 748–2757. https://doi.org/10.1785/0220200484

Polonia, A., Brancolini, G., Torelli, L., & Vera, E. (1999). Structural variability at the active continental margin off southernmost Chile. *Journal of Geodynamics*, *27*(3), 289–307. https://doi.org/10.1016/S0264-3707(98)00003-9

Polonia, A., Torelli, L., Brancolini, G., & Loreto, M.-F. (2007). Tectonic accretion versus erosion along the southern Chile trench: Oblique subduction and margin segmentation. *Tectonics*, *26*(3), TC3005. https://doi.org/10.1029/2006TC001983

Rösler, B., Stein, S., & Spencer, B. D. (2021). Uncertainties in seismic moment tensors inferred from differences between global catalogs. *Seismological Research Letters*, *92*(6), 3698–3711. https://doi.org/10.1785/0220210066

Rösler, B., Stein, S., & Spencer, B. D. (2023). When are non-double-couple components of seismic moment tensors reliable? *Seismica*, *2*(1). https://doi.org/10.26443/seismica.v2i1.241

Rubio, E., Torné, M., Vera, E., & Díaz, A. (2000). Crustal structure of the southernmost Chilean margin from seismic and gravity data. *Tectonophysics*, *323*(1–2), 39–60. https://doi.org/10.1016/S0040-1951(00)00101-3

Stevens, D. E., McNeill, L. C., Henstock, T. J., Barnes, P. M., Crutchley, G., Bangs, N., et al. (2024). Structural variation along the Southern Hikurangi subduction Zone, aotearoa New Zealand, from seismic reflection and retro-deformation analysis. *Tectonics*, *43*(7), e2023TC008212. https://doi.org/10.1029/2023TC008212

Strasser, F. O., Arango, M. C., & Bommer, J. J. (2010). Scaling of the source dimensions of interface and intraslab subduction-zone earthquakes with moment magnitude. *Seismological Research Letters*, *81*(6), 941–950. https://doi.org/10.1785/gssrl.81.6.941

Thomas, C., Livermore, R., & Pollitz, F. (2003). Motion of the Scotia Sea plates. *Geophysical Journal International*, *155*(3), 789–804. https://doi.org/10.1111/j.1365-246X.2003.02069.x

Vuan, A., Russi, M., & Panza, G. (2000). Group velocity tomography in the subantarctic Scotia Sea Region. *Pure and Applied Geophysics*, *157*(9), 1337–1357. https://doi.org/10.1007/PL00001122

Wallace, L. M., Barnes, P., Beavan, J., Van Dissen, R., Litchfield, N., Mountjoy, J., et al. (2012). The kinematics of a transition from subduction to strike-slip: An example from the central New Zealand plate boundary. *Journal of Geophysical Research*, *117*(B2), B02405. https://doi.org/10.1029/2011JB008640

Woollam, J., Münchmeyer, J., Tilmann, F., Rietbrock, A., Lange, D., Bornstein, T., et al. (2022). SeisBench—A toolbox for machine learning in seismology. *Seismological Research Letters*, *93*(3), 1695–1709. https://doi.org/10.1785/0220210324

19448007, 2026, 20, Downloaded from https://agupubs.onlinelibrary.wiley.com/doi/10.1029/2026GL122178 by Alessandro Vuan - Ogs Trieste Istituto Nazionale , Wiley Online Library on [13/10/2026]. See the Terms and Conditions (https://onlinelibrary.wiley.com/terms-and-conditions) on Wiley Online Library for rules of use; OA articles are governed by the applicable Creative Commons License